JACS
JOURNAL OF THE AMERICAN CHEMICAL SOCIETY
pubs.acs.org/JACS
Communication

Optimization of Pore-Space-Partitioned Metal–Organic Frameworks Using the Bioisosteric Concept

Huajun Yang, Yichong Chen, Candy Dang, Anh N. Hong, Pingyun Feng,* and Xianhui Bu*

Cite This: J. Am. Chem. Soc. 2022, 144, 20221–20226
Read Online
ACCESS | Metrics & More | Article Recommendations | Supporting Information

ABSTRACT: Pore space partitioning (PSP) is methodically suited for dramatically increasing the density of guest binding sites, leading to the partitioned acs (pacs) platform capable of record-high uptake for CO_2 and small hydrocarbons such as C_2H_x. For gas separation, achieving high selectivity amid PSP-enabled high uptake offers an enticing prospect. Here we aim for high selectivity by introducing the bioisosteric (BIS) concept, a widely used drug design strategy, into the realm of pore-space-partitioned MOFs. New pacs materials have high C_2H_2/CO_2 selectivity of up to 29, high C_2H_2 uptake of up to 144 cm^3/g (298 K, 1 atm), and high separation potential of up to 5.3 mmol/g, leading to excellent experimental breakthrough performance. These metrics, coupled with exceptional tunability, high stability, and low regeneration energy, demonstrate the broad potential of the BIS-PSP strategy.

Because of the prevalence of aromatic rings in small-molecule drugs, bioisosteric replacement (BIS), commonly practiced by replacing benzene rings with other scaffolds, has become an important method in drug design.[1] Given the similar prevalence of aromatic rings in framework materials (e.g., metal–organic frameworks (MOFs), covalent organic frameworks, and hydrogen-bonded organic frameworks), leveraging the BIS strategy for framework materials design has the potential to further vitalize their development.[2−6] There have been sporadic examples in which benzene rings were replaced by aliphatic moieties on platforms including MOF-5 and UiO-66.[7−9] However, the purposeful design of framework materials leveraging the BIS strategy and its large toolbox and database has yet to start.[10−13]

The application of the BIS strategy in framework materials faces an extra hurdle because in addition to the design of molecular bioisosteres, the additional step of framework formation poses a challenge for bioisostere incorporation. With this in mind, we aim to identify platforms with a built-in structure-directing effect that can guide bioisosteres into intended structures. Here, by integrating pore space partitioning (PSP) with the BIS strategy (Scheme 1), we show that partitioned acs (pacs) is an ideal platform for leveraging the BIS strategy due to synergistic effects among its modules, ultrahigh chemical and geometrical tunability, and high stability.[14,15]

The pacs platform is built from a pore-partitioning agent (denoted L2) and the acs-type MIL-88/MOF-235 framework made from ligand L1 and metal trimers. Of relevance to the BIS strategy is the observed strong interdependent structure-directing effects between L1–trimer and L2–trimer formation.[16−18] As a result, the pacs platform is exceptionally accommodative of variations in L1 or L2 (and in the trimers as well) and therefore provides unparalleled opportunities for implementing the BIS strategy. It should be noted that the BIS strategy is best applied to edit chemical systems that already show promising properties for targeted applications. Such is

Scheme 1. (A) Size Range of sp^2-L1 Ligands in Pacs (Ligands Are Shown with Substituents Omitted); (B) BIS Strategy in Drug Design and Its Parallel in Framework Materials Design

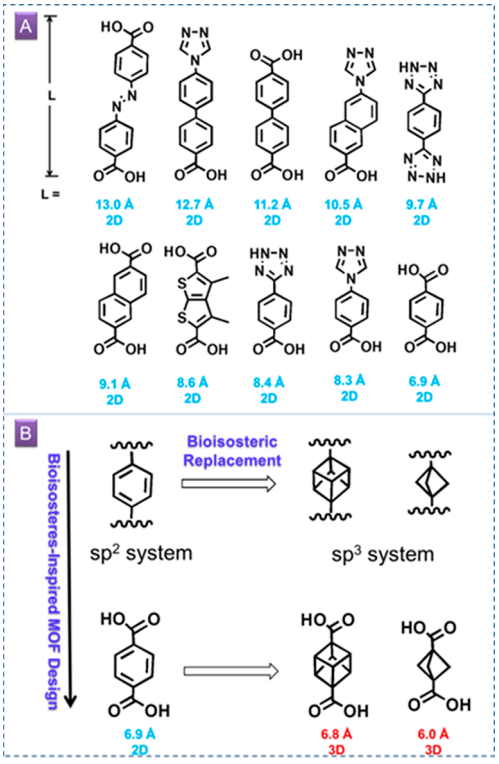

Received: September 1, 2022
Published: October 28, 2022

https://doi.org/10.1021/jacs.2c09349
J. Am. Chem. Soc. 2022, 144, 20221–20226

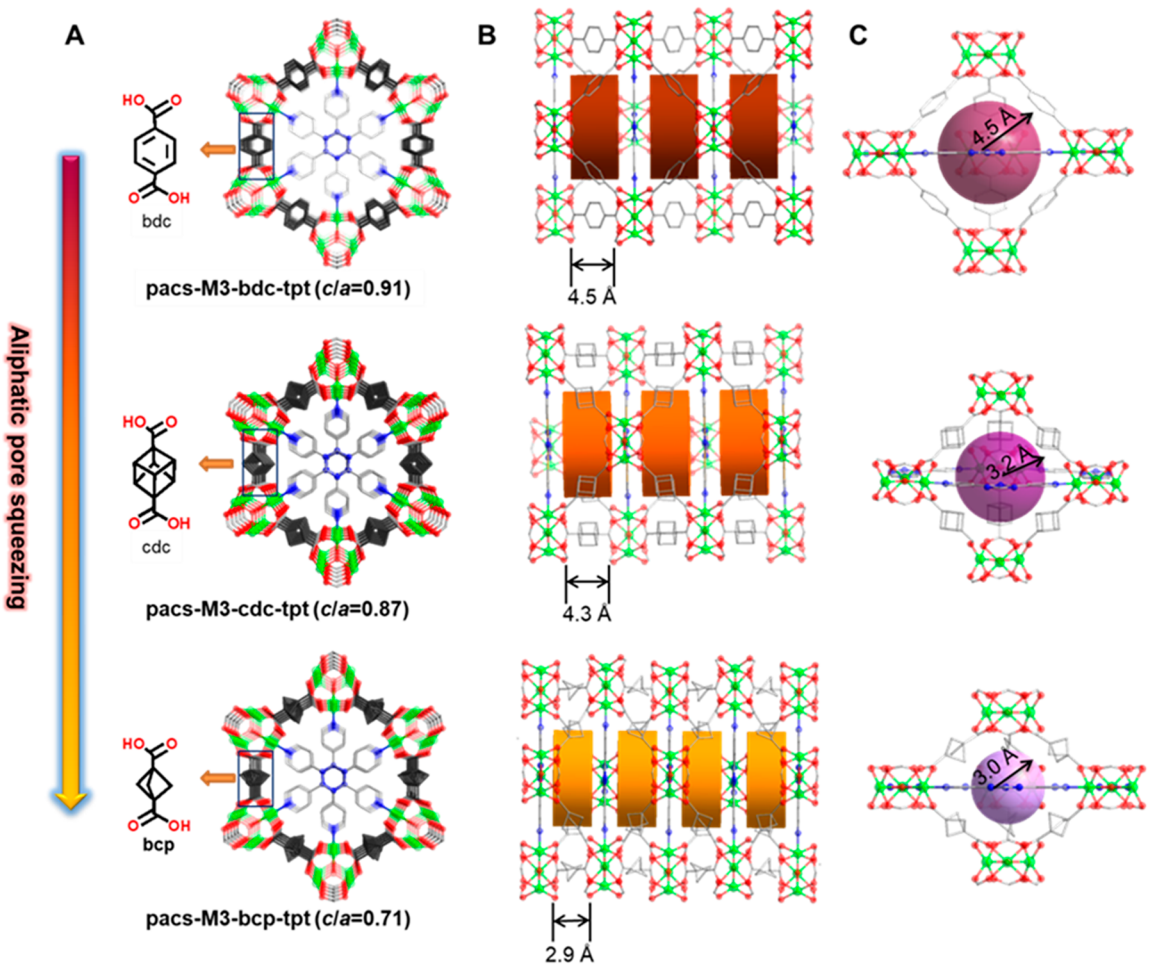

Figure 1. Comparison between pacs-M_3-L1-tpt materials (L1 = bdc, cdc, bcp). (A) Views along the *c* axis. The *c*/*a* ratios were calculated from the Ni_3 compositions. (B) Side views of hexagonal cylinder pores. (C) Side views of trigonal-bipyramidal pores. Color code: green, Ni; red, O; blue, N; gray, C. The distances in (B) and (C) exclude the van der Waals radii of surface atoms.

the case for pacs because the PSP strategy, intrinsic to pacs platform, has led to near- or at-record-high gas (e.g., C_2H_x) uptake capacities.[19−21] With such well-established uptake and high stability, we are intrigued by the prospect that the integration of BIS and PSP may offer a solution to yet another critical parameter in gas separation: selectivity.

To date, L1 ligands in reported pacs are sp^2-based, with the smallest L1 being terephthalate (bdc). In medicinal chemistry, it has been discovered that bioisosteric replacement using bioisosteres with increased 3-D character can lead to decreased nonspecific binding. This effect can be similarly explored in MOFs to help improve gas selectivity. The ligand 3-D character can be measured with the F_{sp^3} value (the ratio of the number of sp^3 carbons to the total number of carbons). In the past decade, the pursuit of 3-D cyclic scaffolds in drug design has led to the wide use of bicyclo[1.1.1]pentane (bcp) as a bioisostere for para-substituted benzene rings.[22,23] In addition to its 3-D character, bcp is extreme because it is the smallest bridged bicyclic ring (only ∼1.87 Å between bridgehead carbons, compared with 2.79 Å between the para positions in benzene).

In this work, bicyclo[1.1.1]pentane-1,3-dicarboxylic acid (H_2bcp) and cubane-1,4-dicarboxylic acid (H_2cdc) were used to build pacs using the BIS-PSP strategy. Among sp^3 bioisosteres, bcp (C_5H_8), cubane (C_8H_8), and bicyclo[2.2.2]-octane (C_8H_{14}) are among the best for their match with the para substitution pattern of the benzene ring. They are able to serve the same scaffolding role as the benzene ring and yet engage in different electronic and steric interactions with targets. Two series of pacs materials are reported here: CPM-111 from bcp and CPM-125 from cdc. Ultramicropores (∼5.9 Å) were achieved with bcp, together with multifold enhancement of the C_2H_2/CO_2 and C_3H_6/C_3H_8 selectivities. CPM-111a-Ni (i.e., Ni_3-bcp-tpt) is an excellent adsorbent in terms of key separation metrics, including high selectivity, high gravimetric and volumetric uptake, easy regeneration, and high stability.

Even with just bcp and cdc as L1 ligands, many new pacs materials are accessible using diverse trimers and L2 ligands. Here we synthesized nine representative materials from five types of trimers (Ni_3, Co_3, Mg_3, Co_xV_{3-x}, and Ni_xV_{3-x}) and two types of L2 ligands (tpt = 2,4,6-tris(4-pyridyl)-1,3,5-triazine) and tppy = 2,4,6-tris(4-pyridyl)pyridine). Pure Ni_3-bdc-tpt (CPM-33a) was synthesized for comparison (Tables S1−S5).

The bcp family expands the known lower limit of the L1/L2 length ratio and the related unit-cell *c*/*a* ratio. These ratios are important parameters of the pacs platform and control the pore shape and size. All new pacs materials have nearly the same *a* length (∼16.9 Å) as bdc-pacs because the *a* axis is

https://doi.org/10.1021/jacs.2c09349
J. Am. Chem. Soc. 2022, 144, 20221−20226

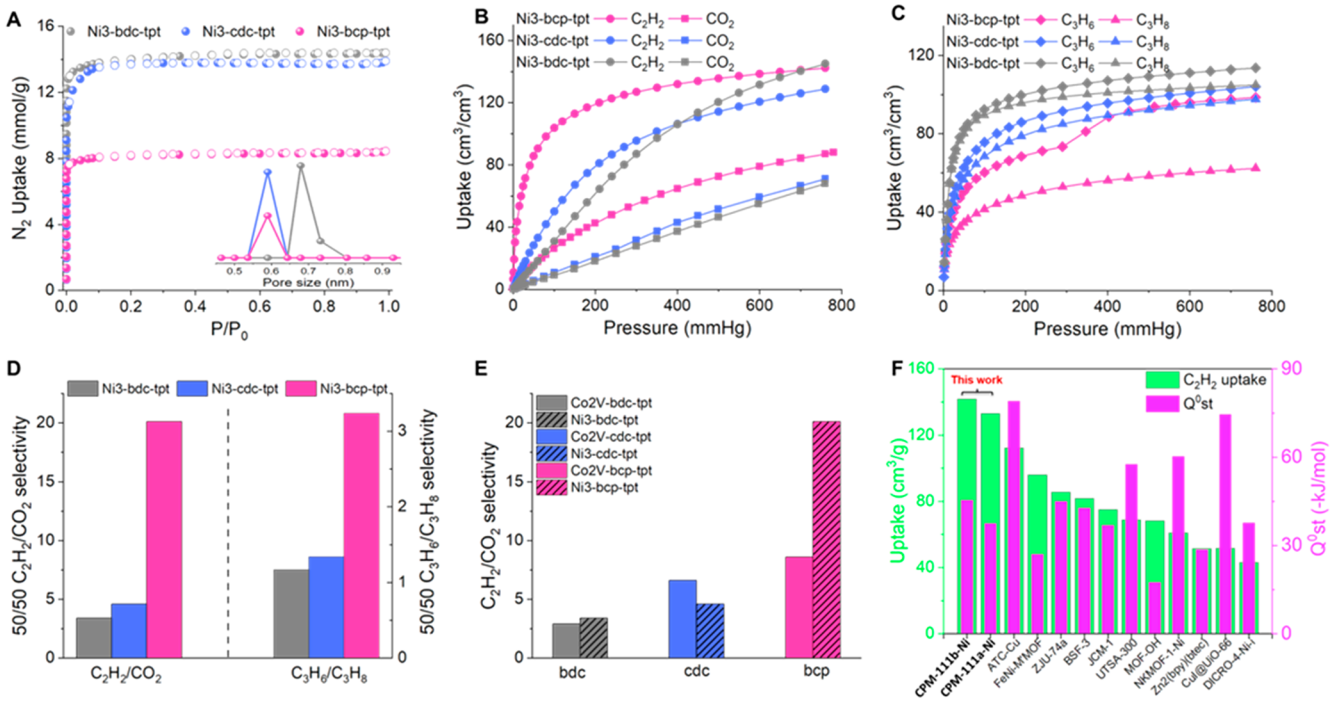

Figure 2. Various comparisons of (A) N_2 adsorption isotherms and DFT pore size distributions, (B) C_2H_2 and CO_2 adsorption isotherms at 298 K, (C) C_3H_6 and C_3H_8 adsorption isotherms at 298 K, (D) 50/50 C_2H_2/CO_2 and C_3H_6/C_3H_8 selectivities for different L1 ligands, (E) C_2H_2/CO_2 selectivities between Ni_3 and Co_2V trimers, and (F) C_2H_2 uptakes (298 K and 1 atm) and Q_{st}^0 values for top-performing MOFs with C_2H_2/CO_2 selectivity > 12.

primarily determined by L2. However, the *c* length is significantly reduced in bcp-pacs (from 15.2 to 12.1 Å), leading to a *c*/*a* ratio of 0.71, the lowest reported to date.[24]

Bioisosteric replacement in pacs (bdc → cdc → bcp) leads to stepwise control over the pore size and pore surface area. The cdc ligand is slightly shorter than bdc (2.72 Å between the bridgehead carbons in cdc vs 2.79 Å between the para positions in benzene) but has a 3-D shape with two extra CH groups. The pore dimensions measured between metal trimer nodes barely change in going from bdc to cdc, but the accessible pore space is smaller due to the sp^3 L1 ligand. In particular, while the height of the hexagonal pores shows only a slight decrease (4.5 to 4.3 Å) in going from bdc to cdc, the inner radius of the trigonal-bipyramidal pores decreases from 4.5 to 3.2 Å. In going from bdc to bcp, both types of pores are compressed significantly along the *c* axis. The height of the hexagonal pores is reduced to 2.9 Å, a 35% decrease from bdc-pacs, while the radius of the trigonal-bipyramidal pores decreases to 3.0 Å (Figure 1). Correspondingly, the guest-accessible volume ratio calculated from PLATON decreases from 58.1% in Ni_3-bdc-tpt to 53.5% in Ni_3-cdc-tpt and 33.0% in Ni_3-bcp-tpt.

The pore shrinkage in going from bdc to cdc and bcp was confirmed by isotherms (Figure 2A). DFT-calculated pore size distributions showed that pore sizes of Ni_3-cdc-tpt and Ni_3-bcp-tpt are centered around 5.9 Å (ultramicropores). This is in contrast to 6.8 Å for Ni_3-bdc-tpt. The short and bulky bcp also leads to a significant reduction in Brunauer−Emmett−Teller (BET) surface area (Table S6).

The adsorption properties of two gas pairs (C_2H_2/CO_2 and C_3H_6/C_3H_8) were studied (Figures S5−S12). These pacs materials showed efficient C_2H_2/CO_2 separation performance (Figure 2B). The gravimetric C_2H_2 uptakes at 298 K and 1 atm were 133.0, 130.7, and 162.1 cm^3/g for Ni_3-bcp-tpt, Ni_3-cdc-tpt, and Ni_3-bdc-tpt, respectively, corresponding to volumetric uptakes of 142.3, 128.7, and 144.9 cm^3/cm^3. Despite the smaller size of bcp, the decrease in C_2H_2 uptake is minor in going from Ni_3-bdc-tpt to Ni_3-bcp-tpt and is negligible for the volumetric uptake. This indicates more efficient pore use and a higher packing density of C_2H_2 in Ni_3-bcp-tpt. The C_2H_2 packing density of Ni_3-bcp-tpt is 0.5 g/cm^3. This value is among the highest in MOFs and is 73% higher than that of Ni_3-bdc-tpt (0.29 g/cm^3).[25−27] It should be noted that the actual packing density could be higher because the pore volume is overestimated due to omission of guest cations in the calculation (Figures S13 and S14).

The improvement in the C_3H_6/C_3H_8 separation in going from bdc and cdc to bcp is profound (Figure 2C). Ni_3-bdc-tpt and Ni_3-cdc-tpt could barely separate them due to the similar C_3H_6 and C_3H_8 isotherms. In comparison, there is a big gap between the C_3H_6 and C_3H_8 adsorption isotherms for Ni_3-bcp-tpt. Also interesting is the observation of flexible-robust behavior in the C_3H_6 adsorption isotherm with an uptake jump at around 300 mmHg.[28,29] This gating behavior could be related to molecular dynamics of bcp such as rotation of the bicyclic ring upon target binding.[11,30]

Ideal adsorbed solution theory (IAST) selectivity calculations confirmed the dramatic enhancement upon bioisosteric replacement with bcp (Figure 2D). Ni_3-bcp-tpt shows a high C_2H_2/CO_2 selectivity of 20.1 at 298 K and 1 bar, about 6 times that of its bdc counterpart. There is also a 177% increase in C_3H_6/C_3H_8 selectivity from Ni_3-bdc-tpt to Ni_3-bcp-tpt. Notably, the C_2H_2/CO_2 selectivity for Ni_3-bcp-tpt is higher than those for many top-performing MOFs, such as JCM-1 (13.7), DICRO-4-Ni-i (13.9), and BSF-3 (16.3), and is especially remarkable among MOFs with high C_2H_2 uptake.[31−33] The higher performance of the materials based on sp^3 ligands is likely due to the smaller pores and the extra

https://doi.org/10.1021/jacs.2c09349
J. Am. Chem. Soc. 2022, 144, 20221−20226

hydrogen atoms on the ligand surface, which can provide more interaction sites, especially for gases that can act as hydrogen acceptors (e.g., C_2H_2 with $C^{\delta-}$).

Significantly, the ultramicropore environment of bcp-based frameworks amplifies the impact of other structural variations on the separation performance. In going from the neutral Co_2V-based framework to the anionic Ni_3-based framework, the C_2H_2/CO_2 selectivities are comparable for bdc- and cdc-based pacs. However, there is a dramatic improvement in selectivity (134% increase) in going from Co_2V-bcp-tpt to Ni_3-bcp-tpt (from 8.6 to 20.1). Changing Ni to Mg also leads to a dramatic 44% increase in the selectivity from 20.1 to 29.0 (Figure 2E). Furthermore, while the replacement of tpt by tppy shows little influence on the separation performance in bdc-pacs, it has a significant impact on the C_2H_2/CO_2 selectivity in bcp-pacs (Table S7).

To highlight the success of the BIS-PSP strategy, we compare the high selectivities and high uptakes of the new bcp-based pacs materials with those of top-performing MOFs. Among MOFs with high C_2H_2/CO_2 selectivity (>12), Ni_3-bcp-tpt and Ni_3-bcp-tppy likely have the highest C_2H_2 uptakes at both 0.1 bar and 1 atm (Figure 2F).[34−36] Among MOFs with higher or comparable C_2H_2 uptakes for C_2H_2/CO_2 separation, Ni_3-bcp-tpt has much higher selectivity (Table S8). The separation potential, which is a metric incorporating the influence of both selectivity and uptake, is used to evaluate separation performance.[37,38] The bcp pacs materials show very high separation potentials ranging from 4.4 to 5.3 mmol/g. The pacs-Mg_3-bcp-tpt material has the highest separation potential in this series, 5.3 mmol/g, which is higher than those of previous benchmark pacs MOFs (FJU-90 and SNNU-27).[39−42] The breakthrough experiments showed that Ni_3-bcp-tpt had a long breakthrough time and excellent separation performance (Figure S15).

The bcp pacs materials also feature a low adsorption enthalpy, which is highly desirable due to reduced energy consumption for regeneration. The isosteric heat of adsorption at near-zero coverage (Q_{st}^0), calculated from adsorption isotherms at 273 and 298 K, is 37.5 kJ/mol for Ni_3-bcp-tpt. This value is quite small among MOFs with high C_2H_2/CO_2 selectivity, such as ATC-Cu (79.1 kJ/mol) and NKMOF-1 (60.3 kJ/mol).[43−46] The easy regeneration of Ni_3-bcp-tpt was confirmed by multiple cycles of gas adsorption experiments. The framework was found to show no capacity loss in five cycles and needed only mild reactivation conditions (60 °C for 30 min) (Figure S16).

In addition to excellent sorption performance, Ni_3-bcp-tpt has high chemical stability compared with aromatic Ni_3-bdc-tpt as well as other top-performing MOFs for C_2H_2/CO_2 separation. Powder X-ray diffraction confirmed that Ni_3-bcp-tpt maintained its crystallinity after being soaked in water for 24 h. In comparison, diffraction peak broadening was observed in Ni_3-bdc-tpt (Figure S17). The stability difference was further shown by gas adsorption. N_2 adsorption at 77 K showed a large decrease in surface area for Ni_3-bdc-tpt after water treatment as well as a defect-related hysteresis loop (Figure S18). In comparison, there was only minor surface area decrease for Ni_3-bcp-tpt. C_2H_2 adsorption confirmed the stability difference observed in N_2 adsorption. Water treatment caused a 47.3% loss of C_2H_2 uptake for Ni_3-bdc-tpt, while the loss was only 7.7% for Ni_3-bcp-tpt (Figure 3).

In conclusion, by integrating the bioisosteric replacement strategy with pore space partitioning, we successfully synthesized a family of ultramicroporous materials with much-enhanced gas separation properties and chemical stability. While this work has already demonstrated high gas separation potentials, the generality of the BIS-PSP method promises even further optimization of other MOF platforms as well as other types of framework materials.

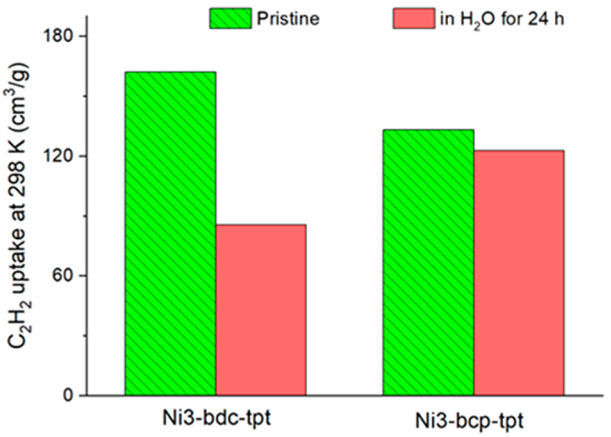

Figure 3. Comparison of hydrothermal stability between Ni3-bdc-tpt and Ni3-bcp-tpt based on C_2H_2 uptake at 298 K.

■ ASSOCIATED CONTENT

Supporting Information

The Supporting Information is available free of charge at https://pubs.acs.org/doi/10.1021/jacs.2c09349.

Experimental procedures and compound characterization data (PDF)

Accession Codes

CCDC 2159091−2159094 contain the supplementary crystallographic data for this paper. These data can be obtained free of charge via www.ccdc.cam.ac.uk/data_request/cif, or by emailing data_request@ccdc.cam.ac.uk, or by contacting The Cambridge Crystallographic Data Centre, 12 Union Road, Cambridge CB2 1EZ, U.K.; fax: +44 1223 336033.

■ AUTHOR INFORMATION

Corresponding Authors

Xianhui Bu − *Department of Chemistry and Biochemistry, California State University, Long Beach, California 90840, United States;* orcid.org/0000-0002-2994-4051; Email: xianhui.bu@csulb.edu

Pingyun Feng − *Department of Chemistry, University of California, Riverside, California 92521, United States;* orcid.org/0000-0003-3684-577X; Email: pingyun.feng@ucr.edu

Authors

Huajun Yang − *Department of Chemistry and Biochemistry, California State University, Long Beach, California 90840, United States; Department of Chemistry, University of California, Riverside, California 92521, United States;* orcid.org/0000-0002-4664-4042

Yichong Chen − *Department of Chemistry, University of California, Riverside, California 92521, United States*

Candy Dang − *Department of Chemistry and Biochemistry, California State University, Long Beach, California 90840, United States*

Anh N. Hong − *Department of Chemistry, University of California, Riverside, California 92521, United States;* orcid.org/0000-0003-1808-5527

Complete contact information is available at: https://pubs.acs.org/10.1021/jacs.2c09349

Notes

The authors declare no competing financial interest.

■ ACKNOWLEDGMENTS

The gas separation studies were supported by the U.S. Department of Energy, Office of Basic Energy Sciences, Materials Sciences and Engineering Division, under Award DE-SC0010596 (P.F.). X.B. thanks NSF (DMR 2105961) for synthetic and single-crystal X-ray studies and CSULB for 3 units of teaching release time.

■ REFERENCES

(1) Subbaiah, M. A. M.; Meanwell, N. A. Bioisosteres of the Phenyl Ring: Recent Strategic Applications in Lead Optimization and Drug Design. *J. Med. Chem.* **2021**, *64*, 14046−14128.

(2) Furukawa, H.; Cordova, K. E.; O'Keeffe, M.; Yaghi, O. M. The Chemistry and Applications of Metal-Organic Frameworks. *Science* **2013**, *341*, 1230444.

(3) Sumida, K.; Rogow, D. L.; Mason, J. A.; McDonald, T. M.; Bloch, E. D.; Herm, Z. R.; Bae, T.-H.; Long, J. R. Carbon Dioxide Capture in Metal-Organic Frameworks. *Chem. Rev.* **2012**, *112*, 724−781.

(4) Lin, R.-B.; Zhang, Z.; Chen, B. Achieving High Performance Metal-Organic Framework Materials through Pore Engineering. *Acc. Chem. Res.* **2021**, *54*, 3362−3376.

(5) Yuan, S.; Feng, L.; Wang, K.; Pang, J.; Bosch, M.; Lollar, C.; Sun, Y.; Qin, J.; Yang, X.; Zhang, P.; Wang, Q.; Zou, L.; Zhang, Y.; Zhang, L.; Fang, Y.; Li, J.; Zhou, H.-C. Stable Metal-Organic Frameworks: Design, Synthesis, and Applications. *Adv. Mater.* **2018**, *30*, 1704303.

(6) Yang, L.; Qian, S.; Wang, X.; Cui, X.; Chen, B.; Xing, H. Energy-efficient separation alternatives: metal-organic frameworks and membranes for hydrocarbon separation. *Chem. Soc. Rev.* **2020**, *49*, 5359−5406.

(7) Macreadie, L. K.; Mensforth, E. J.; Babarao, R.; Konstas, K.; Telfer, S. G.; Doherty, C. M.; Tsanaktsidis, J.; Batten, S. R.; Hill, M. R. CUB-5: A Contoured Aliphatic Pore Environment in a Cubic Framework with Potential for Benzene Separation Applications. *J. Am. Chem. Soc.* **2019**, *141*, 3828−3832.

(8) Slyusarchuk, V. D.; Kruger, P. E.; Hawes, C. S. Cyclic Aliphatic Hydrocarbons as Linkers in Metal-Organic Frameworks: New Frontiers for Ligand Design. *ChemPlusChem* **2020**, *85*, 845−854.

(9) Bueken, B.; Vermoortele, F.; Cliffe, M. J.; Wharmby, M. T.; Foucher, D.; Wieme, J.; Vanduyfhuys, L.; Martineau, C.; Stock, N.; Taulelle, F.; Van Speybroeck, V.; Goodwin, A. L.; De Vos, D. A Breathing Zirconium Metal-Organic Framework with Reversible Loss of Crystallinity by Correlated Nanodomain Formation. *Chem. - Eur. J.* **2016**, *22*, 3264−3267.

(10) Macreadie, L. K.; Babarao, R.; Setter, C. J.; Lee, S. J.; Qazvini, O. T.; Seeber, A. J.; Tsanaktsidis, J.; Telfer, S. G.; Batten, S. R.; Hill, M. R. Enhancing Multicomponent Metal-Organic Frameworks for Low Pressure Liquid Organic Hydrogen Carrier Separations. *Angew. Chem., Int. Ed.* **2020**, *59*, 6090−6098.

(11) Perego, J.; Bracco, S.; Negroni, M.; Bezuidenhout, C. X.; Prando, G.; Carretta, P.; Comotti, A.; Sozzani, P. Fast motion of molecular rotors in metal-organic framework struts at very low temperatures. *Nat. Chem.* **2020**, *12*, 845−851.

(12) Fairley, M.; Gilson, S. E.; Hanna, S. L.; Mishra, A.; Knapp, J. G.; Idrees, K. B.; Chheda, S.; Traustason, H.; Islamoglu, T.; Burns, P. C.; Gagliardi, L.; Farha, O. K.; LaVerne, J. A. Linker Contribution toward Stability of Metal-Organic Frameworks under Ionizing Radiation. *Chem. Mater.* **2021**, *33*, 9285−9294.

(13) Chang, M.; Zhao, Y.; Liu, D.; Yang, J.; Li, J.; Zhong, C. Methane-trapping metal-organic frameworks with an aliphatic ligand for efficient CH_4/N_2 separation. *Sustainable Energy Fuels* **2020**, *4*, 138−142.

(14) Zheng, S.-T.; Zhao, X.; Lau, S.; Fuhr, A.; Feng, P.; Bu, X. Entrapment of Metal Clusters in Metal-Organic Framework Channels by Extended Hooks Anchored at Open Metal Sites. *J. Am. Chem. Soc.* **2013**, *135*, 10270−10273.

(15) Zhao, X.; Bu, X.; Zhai, Q.-G.; Tran, H.; Feng, P. Pore Space Partition by Symmetry-Matching Regulated Ligand Insertion and Dramatic Tuning on Carbon Dioxide Uptake. *J. Am. Chem. Soc.* **2015**, *137*, 1396−1399.

(16) Zhai, Q.-G.; Bu, X.; Zhao, X.; Li, D.-S.; Feng, P. Pore Space Partition in Metal-Organic Frameworks. *Acc. Chem. Res.* **2017**, *50*, 407−417.

(17) Zhao, X.; Bu, X.; Nguyen, E. T.; Zhai, Q.-G.; Mao, C.; Feng, P. Multivariable Modular Design of Pore Space Partition. *J. Am. Chem. Soc.* **2016**, *138*, 15102−15105.

(18) Yang, H.; Peng, F.; Hong, A. N.; Wang, Y.; Bu, X.; Feng, P. Ultrastable High-Connected Chromium Metal-Organic Frameworks. *J. Am. Chem. Soc.* **2021**, *143*, 14470−14474.

(19) Yang, H.; Wang, Y.; Krishna, R.; Jia, X.; Wang, Y.; Hong, A. N.; Dang, C.; Castillo, H. E.; Bu, X.; Feng, P. Pore-Space-Partition-Enabled Exceptional Ethane Uptake and Ethane-Selective Ethane-Ethylene Separation. *J. Am. Chem. Soc.* **2020**, *142*, 2222−2227.

(20) Wang, Y.; Jia, X.; Yang, H.; Wang, Y.; Chen, X.; Hong, A. N.; Li, J.; Bu, X.; Feng, P. A Strategy for Constructing Pore-Space-Partitioned MOFs with High Uptake Capacity for C_2 Hydrocarbons and CO_2. *Angew. Chem., Int. Ed.* **2020**, *59*, 19027−19030.

(21) Zhai, Q.-G.; Bu, X.; Mao, C.; Zhao, X.; Daemen, L.; Cheng, Y.; Ramirez-Cuesta, A. J.; Feng, P. An ultra-tunable platform for molecular engineering of high-performance crystalline porous materials. *Nat. Commun.* **2016**, *7*, 13645.

(22) Stepan, A. F.; Subramanyam, C.; Efremov, I. V.; Dutra, J. K.; O'Sullivan, T. J.; DiRico, K. J.; McDonald, W. S.; Won, A.; Dorff, P. H.; Nolan, C. E.; Becker, S. L.; Pustilnik, L. R.; Riddell, D. R.; Kauffman, G. W.; Kormos, B. L.; Zhang, L.; Lu, Y.; Capetta, S. H.; Green, M. E.; Karki, K.; Sibley, E.; Atchison, K. P.; Hallgren, A. J.; Oborski, C. E.; Robshaw, A. E.; Sneed, B.; O'Donnell, C. J. Application of the Bicyclo[1.1.1]pentane Motif as a Nonclassical Phenyl Ring Bioisostere in the Design of a Potent and Orally Active γ-Secretase Inhibitor. *J. Med. Chem.* **2012**, *55*, 3414−3424.

(23) Kanazawa, J.; Uchiyama, M. Recent Advances in the Synthetic Chemistry of Bicyclo[1.1.1]pentane. *Synlett* **2019**, *30*, 1−11.

(24) Hong, A. N.; Yang, H.; Li, T.; Wang, Y.; Wang, Y.; Jia, X.; Zhou, A.; Kusumoputro, E.; Li, J.; Bu, X.; Feng, P. Pore-Space Partition and Optimization for Propane-Selective High-Performance Propane/Propylene Separation. *ACS Appl. Mater. Interfaces* **2021**, *13*, 52160−52166.

(25) Pei, J.; Wen, H.-M.; Gu, X.-W.; Qian, Q.-L.; Yang, Y.; Cui, Y.; Li, B.; Chen, B.; Qian, G. Dense Packing of Acetylene in a Stable and Low-Cost Metal-Organic Framework for Efficient C_2H_2/CO_2 Separation. *Angew. Chem., Int. Ed.* **2021**, *60*, 25068−25074.

(26) Gong, W.; Cui, H.; Xie, Y.; Li, Y.; Tang, X.; Liu, Y.; Cui, Y.; Chen, B. Efficient C_2H_2/CO_2 Separation in Ultramicroporous Metal-Organic Frameworks with Record C_2H_2 Storage Density. *J. Am. Chem. Soc.* **2021**, *143*, 14869−14876.

(27) Zhang, X.; Lin, R.-B.; Wu, H.; Huang, Y.; Ye, Y.; Duan, J.; Zhou, W.; Li, J.-R.; Chen, B. Maximizing acetylene packing density for highly efficient C_2H_2/CO_2 separation through immobilization of amine sites within a prototype MOF. *Chem. Eng. J.* **2022**, *431*, 134184.

(28) Li, L.; Lin, R.-B.; Krishna, R.; Wang, X.; Li, B.; Wu, H.; Li, J.; Zhou, W.; Chen, B. Flexible-Robust Metal-Organic Framework for Efficient Removal of Propyne from Propylene. *J. Am. Chem. Soc.* **2017**, *139*, 7733−7736.

(29) Wang, J.; Zhang, Y.; Zhang, P.; Hu, J.; Lin, R.-B.; Deng, Q.; Zeng, Z.; Xing, H.; Deng, S.; Chen, B. Optimizing Pore Space for

Flexible-Robust Metal-Organic Framework to Boost Trace Acetylene Removal. *J. Am. Chem. Soc.* **2020**, *142*, 9744−9751.
(30) Perego, J.; Bezuidenhout, C. X.; Bracco, S.; Prando, G.; Marchiò, L.; Negroni, M.; Carretta, P.; Sozzani, P.; Comotti, A. Cascade Dynamics of Multiple Molecular Rotors in a MOF: Benchmark Mobility at a Few Kelvins and Dynamics Control by CO_2. *J. Am. Chem. Soc.* **2021**, *143*, 13082−13090.
(31) Lee, J.; Chuah, C. Y.; Kim, J.; Kim, Y.; Ko, N.; Seo, Y.; Kim, K.; Bae, T. H.; Lee, E. Separation of Acetylene from Carbon Dioxide and Ethylene by a Water-Stable Microporous Metal-Organic Framework with Aligned Imidazolium Groups inside the Channels. *Angew. Chem., Int. Ed.* **2018**, *57*, 7869−7873.
(32) Scott, H. S.; Shivanna, M.; Bajpai, A.; Madden, D. G.; Chen, K.-J.; Pham, T.; Forrest, K. A.; Hogan, A.; Space, B.; Perry, J. J., IV; Zaworotko, M. J. Highly Selective Separation of C_2H_2 from CO_2 by a New Dichromate-Based Hybrid Ultramicroporous Material. *ACS Appl. Mater. Interfaces* **2017**, *9*, 33395−33400.
(33) Zhang, Y.; Hu, J.; Krishna, R.; Wang, L.; Yang, L.; Cui, X.; Duttwyler, S.; Xing, H. Rational Design of Microporous MOFs with Anionic Boron Cluster Functionality and Cooperative Dihydrogen Binding Sites for Highly Selective Capture of Acetylene. *Angew. Chem., Int. Ed.* **2020**, *59*, 17664−17669.
(34) Gao, J.; Qian, X.; Lin, R.-B.; Krishna, R.; Wu, H.; Zhou, W.; Chen, B. Mixed Metal-Organic Framework with Multiple Binding Sites for Efficient C_2H_2/CO_2 Separation. *Angew. Chem., Int. Ed.* **2020**, *59*, 4396−4400.
(35) Pei, J.; Shao, K.; Wang, J.-X.; Wen, H.-M.; Yang, Y.; Cui, Y.; Krishna, R.; Li, B.; Qian, G. A Chemically Stable Hofmann-Type Metal-Organic Framework with Sandwich-Like Binding Sites for Benchmark Acetylene Capture. *Adv. Mater.* **2020**, *32*, 1908275.
(36) Chen, Y.; Du, Y.; Wang, Y.; Krishna, R.; Li, L.; Yang, J.; Li, J.; Mu, B. A stable metal-organic framework with well-matched pore cavity for efficient acetylene separation. *AlChE J.* **2021**, *67*, No. e17152.
(37) Krishna, R. Screening metal-organic frameworks for mixture separations in fixed-bed adsorbers using a combined selectivity/capacity metric. *RSC Adv.* **2017**, *7*, 35724−35737.
(38) Krishna, R. Methodologies for screening and selection of crystalline microporous materials in mixture separations. *Sep. Purif. Technol.* **2018**, *194*, 281−300.
(39) Ye, Y.; Ma, Z.; Lin, R.-B.; Krishna, R.; Zhou, W.; Lin, Q.; Zhang, Z.; Xiang, S.; Chen, B. Pore Space Partition within a Metal-Organic Framework for Highly Efficient C_2H_2/CO_2 Separation. *J. Am. Chem. Soc.* **2019**, *141*, 4130−4136.
(40) Xue, Y.-Y.; Bai, X.-Y.; Zhang, J.; Wang, Y.; Li, S.-N.; Jiang, Y.-C.; Hu, M.-C.; Zhai, Q.-G. Precise Pore Space Partitions Combined with High-Density Hydrogen-Bonding Acceptors within Metal-Organic Frameworks for Highly Efficient Acetylene Storage and Separation. *Angew. Chem., Int. Ed.* **2021**, *60*, 10122−10128.
(41) Ye, Y.; Xian, S.; Cui, H.; Tan, K.; Gong, L.; Liang, B.; Pham, T.; Pandey, H.; Krishna, R.; Lan, P. C.; Forrest, K. A.; Space, B.; Thonhauser, T.; Li, J.; Ma, S. Metal-Organic Framework Based Hydrogen-Bonding Nanotrap for Efficient Acetylene Storage and Separation. *J. Am. Chem. Soc.* **2022**, *144*, 1681−1689.
(42) Di, Z.; Liu, C.; Pang, J.; Chen, C.; Hu, F.; Yuan, D.; Wu, M.; Hong, M. Cage-Like Porous Materials with Simultaneous High C_2H_2 Storage and Excellent C_2H_2/CO_2 Separation Performance. *Angew. Chem., Int. Ed.* **2021**, *60*, 10828−10832.
(43) Niu, Z.; Cui, X.; Pham, T.; Lan, P. C.; Xing, H.; Forrest, K. A.; Wojtas, L.; Space, B.; Ma, S. A Metal-Organic Framework Based Methane Nano-trap for the Capture of Coal-Mine Methane. *Angew. Chem., Int. Ed.* **2019**, *58*, 10138−10141.
(44) Peng, Y.-L.; Pham, T.; Li, P.; Wang, T.; Chen, Y.; Chen, K.-J.; Forrest, K. A.; Space, B.; Cheng, P.; Zaworotko, M. J.; Zhang, Z. Robust Ultramicroporous Metal-Organic Frameworks with Benchmark Affinity for Acetylene. *Angew. Chem., Int. Ed.* **2018**, *57*, 10971−10975.
(45) Zhang, L.; Jiang, K.; Yang, L.; Li, L.; Hu, E.; Yang, L.; Shao, K.; Xing, H.; Cui, Y.; Yang, Y.; Li, B.; Chen, B.; Qian, G. Benchmark C_2H_2/CO_2 Separation in an Ultra-Microporous Metal-Organic Framework via Copper(I)-Alkynyl Chemistry. *Angew. Chem., Int. Ed.* **2021**, *60*, 15995−16002.
(46) Lin, R.-B.; Li, L.; Wu, H.; Arman, H.; Li, B.; Lin, R.-G.; Zhou, W.; Chen, B. Optimized Separation of Acetylene from Carbon Dioxide and Ethylene in a Microporous Material. *J. Am. Chem. Soc.* **2017**, *139*, 8022−8028.

https://doi.org/10.1021/jacs.2c09349
J. Am. Chem. Soc. 2022, 144, 20221−20226